Simultaneous spatial and temporal focusing of femtosecond pulses

Guanghao Zhu, James van Howe, Michael Durst, Warren Zipfel, and Chris Xu

School of Applied and Engineering Physics, Cornell University, Ithaca, N.Y. 14850
cx10@cornell.edu

Abstract: We study and demonstrate the technique of simultaneous spatial and temporal focusing of femtosecond pulses, with the aim to improve the signal-to-background ratio in multiphoton imaging. This concept is realized by spatially separating spectral components of pulses into a "rainbow beam" and recombining these components only at the spatial focus of the objective lens. Thus, temporal pulse width becomes a function of distance, with the shortest pulse width confined to the spatial focus. We developed analytical expressions to describe this method and experimentally demonstrated the feasibility. The concept of simultaneous spatial and temporal focusing of femtosecond pulses has the great potential to significantly reduce the background excitation in multiphoton microscopy, which fundamentally limits the imaging depth in highly scattering biological specimens.

OCIS codes: (170.3880) Medical and biological imaging; (180.6900) Three-dimensional microscopy.

References and links

1. W. Denk, K. R. Delaney, A. Gelperin, D. Kleinfeld, B. W. Strawbridge, D. W. Tank, and R. Yuste, "Anatomical and functional imaging of neurons using 2-photon laser microscopy," J. Neuroscience Methods **54,** 161-162 (1994).
2. J. M. Squirrell, D. L. Wokosin, J. G. White, and B. D. Bavister, "Long-term two-photon fluorescence imaging of mammalian embryos without compromising viability," Nature Biotechnol. **17,** 763-767 (1999).
3. W. R. Zipfel, R. M. Williams, R. Christie, A. Y. Nikitin, B. T. Hyman, and W. W. Webb, "Live tissue intrinsic emission microscopy using multi-photon intrinsic fluorescence and second harmonic generation," Proc. Natl. Acad. Sci. **100,** 7075-7080 (2003).
4. P. Theer, M. T. Hasan, and W. Denk, "Two-photon imaging to a depth 1000um in living brains by use of $Ti:Al_2O_3$ regenerative amplifier," Opt. Lett. **28,** 1022-1024 (2003).
5. During our research work of temporal focusing, we become aware, through the reviewing process, that a manuscript was submitted on a similar concept for wide field imaging. D. Oron, E. Tal and Y. Silberberg, "Scanningless depth-resolved microscopy," Opt. Express **13,** 1468-1476 (2005), http://www.opticsexpress.org/abstract.cfm?URI=OPEX-13-5-1468.
6. H. A. Haus, *Waves and fields in optoelectronics*, (Prentice-Hall, Englewood Cliffs, NJ, 1984)**,** Chap 4.
7. O. E. Martinez, "Grating and prism compressor in the case of finite beam size," J. Opt. Soc. Am. **3,** 929-934, 1986.
8. C. Xu, J. Guild, W. W. Webb and W. Denk, "Determination of absolute two-photon cross sections by in situ second order autocorrelations," Opt. Lett. **20,** 2372-2374 (1995).
9. G.J. Brakenhoff, J. Squier, T. Norris, A.C. Bliton W.H. Wade and B. Athey, "Real-time two-photon confocal microscopy using a femtosecond amplified Ti:sapphire system," J. Microsc. **181**, 253-259 (1996).

1. Introduction

Laser scanning multiphoton microscopy (MPM) has greatly improved the penetration depth of optical imaging and proven to be well suited for a variety of imaging applications deep within intact or semi-intact tissues, such as demonstrated in the studies of neuronal activity and anatomy [1], developing embryos [2], and tissue morphology and pathology [3]. When

#6020 - $15.00 US Received 16 December 2004; revised 23 February 2005; accepted 14 March 2005

compared to one-photon confocal microscopy, a factor of 2 to 3 improvement in penetration depth is attainable in MPM. Nonetheless, MPM has so far been restricted to less than 1mm in depth in brain tissues, even with the heroic effort of employing energetic pulses (~ μJ/pulse) produced by a regenerative amplifier [4].

The intrinsic difficulty of imaging deep into biological tissues is scattering. In the context of multiphoton excitation, the effect of scattering is the reduction of the "imaging" photons (photons that maintain their ballistic trajectories) arriving at the focal volume. The excitation power (P) as a function of the penetration depth (z) obeys the well-known exponential behavior: $P(z) = P(0) \cdot \exp(-z / l_s)$, where l_s is the scattering length of the sample. A constant signal level can obviously be maintained if one compensates the loss of excitation power at the focus by exponentially increasing the excitation power at the sample surface, i.e., by exponentially increasing $P(0)$. However, as the penetration depth increases, the background, which includes all fluorescence that originates outside the focal volume and therefore carries no image information, eventually dominates the detected fluorescence. Because of the exponential decay of the excitation power, the signal-to-background ratio (SBR) decreases to zero at large imaging depth [4]. On the other hand, a minimum SBR is required for a satisfactory imaging performance. Thus, it is the SBR rather than the decreasing signal strength that intrinsically limits the maximum penetration depth in MPM.

It is important to note that being a nonlinear process, the efficiency of multiphoton excitation also strongly depends on the excitation pulse width (τ). For example, the excitation efficiency varies as τ^{-1} for two-photon excited fluorescence. Thus, in addition to the spatial focusing, an extra degree of confinement for the excitation can be achieved if we can create a temporal focus [5] where the pulse width varies along the propagation direction and the shortest pulse is only achieved at the focal point. Such a technique will improve the SBR by reducing the background excitation while maintaining the signal strength. In this paper, we study and demonstrate the technique of simultaneous spatial and temporal focusing of femtosecond pulses, aiming to improve the SBR in multiphoton excitation.

2. Principle of operation and theoretical analysis

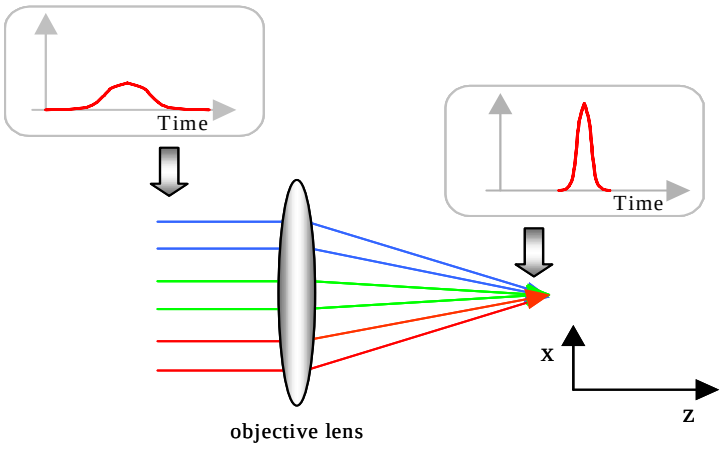

Fig. 1. Schematics for the proposed simultaneous temporal and spatial focusing technique. The system input is a rainbow-like superposition of many parallel optical beams of which the center positions are linearly displaced according to their wavelengths. The spectrum of the input is assumed to be chirp-free. After passing through a regular objective lens, the rainbow beam is then focused and recombined in space. Temporal focusing is achieved because of the reduced spatial overlapping and the non-zero geometric dispersion outside the focal volume.

#6020 - $15.00 US Received 16 December 2004; revised 23 February 2005; accepted 14 March 2005

The basic principle for the simultaneous temporal and spatial focusing is illustrated in Fig. 1. Spatial focusing is still achieved by passing the light through an objective lens. However, instead of keeping all the spectral components well overlapped in space during the focusing process, we propose to first separate them spatially and then recombine them only at the focal point.

To intuitively understand why an extra degree of temporal focusing can be achieved in our proposed scheme, let us first recapitulate how short pulses are generated in ultrafast optics. It is well known that in order to generate the shortest pulses at one particular spatial point, two critical conditions must be satisfied. The first condition requires that all the available spectral components must be completely spatially overlapped. The second condition requires that the entire optical spectrum must be chirp-free. Regarding the first condition, in our proposed scheme it can be seen that the best spatial overlap occurs only at the focal point. Regarding the second condition, if a chirp-free spectrum of the rainbow beam can be produced at the back aperture of the objective lens, then from the optical path argument, the required chirp-free condition can be re-achieved after the objective but only at the focal point. Since the realization of the above two conditions is restricted at the focal volume, it then follows that the temporal focusing effect will occur only at the vicinity of the focal point.

We develop an analytical model for the temporal focusing to supplement the intuitive picture described above. In the following section, the theoretical analysis is based on the Gaussian beam approximation under the paraxial limit. The steps of our calculation are as follows: we first assume that the input beam profile at the back aperture of the objective can be written as a superposition of many monochromatic, spatially transform-limited Gaussian beams, of which the center positions are linearly displaced according to their wavelengths. We further assume that the optical spectrum of the input waveform at the back aperture of the objective is chirp-free and has a Gaussian spectral profile. Then, for each monochromatic Gaussian beam, we calculate the evolution of the spatial beam profile analytically using the standard paraxial propagation method [6,7]. Finally, we evaluate the performance of the simultaneous temporal and spatial focusing by summing up all the monochromatic contributions. It should be noted that from Fig. 1, since the spatial coupling only happens between x and z directions, the dependence of the beam profile on the variable y is therefore dropped in our treatment [7].

Following the steps outlined above, we first write the input beam amplitude $A_1(x,t)$ at the back aperture of the objective lens as a superposition of many spatial Gaussian beams, of which the center positions are linearly displaced according to their wavelengths,

$$A_1(x,t) = \int_{-\infty}^{+\infty} \exp[-\frac{(x-\alpha\cdot\Delta\omega)^2}{s^2}]\cdot\exp[-\frac{\Delta\omega^2}{\Omega^2}+i\Delta\omega t]\cdot d\Delta\omega, \qquad (1)$$

where $\Delta\omega$ is the offset frequency from the center of the input spectrum, $\sqrt{2\ln 2}\cdot\Omega$ is the FWHM bandwidth of the input spectrum, $\sqrt{2\ln 2}\cdot s$ is the FWHM diameter of each monochromatic beam, α is a proportionality constant and $\alpha\cdot\Delta\omega$ is the linear displacement of the beam center at the offset frequency of $\Delta\omega$. Because we have assumed the input beam profile is a superposition of many spatially transform-limited and temporally chirp-free beams, both Ω and s are then treated as real numbers in our calculations.

We now focus on the calculation of Gaussian beam propagation for one particular monochromatic component $\exp[-(x-\alpha\cdot\Delta\omega)^2/s^2]$. After passing through the objective, the output spatial profile is then modified to $\exp[-(x-\alpha\cdot\Delta\omega)^2/s^2]\cdot\exp(ikx^2/2f)$, where k is the wave vector, and f is the focal length of the objective [6]. Defining the position of the objective as $z=0$, under the paraxial approximation, the diffraction effect can be then modeled in the spatial frequency (k_x) domain as the spatial dispersion $\exp(ik_x^2 z/2k)$ [6]. After Fourier transforming $\exp[-(x-\alpha\cdot\Delta\omega)^2/s^2]\cdot\exp(ikx^2/2f)$ into the k_x domain,

#6020 - $15.00 US Received 16 December 2004; revised 23 February 2005; accepted 14 March 2005

multiplying the result by the spatial dispersion $\exp(ik_x^2 \cdot z/2k)$, and then inversely Fourier transforming the product back to real space, the diffracted spatial beam amplitude $M(x,z,\Delta\omega)$ is calculated as

$$M(x,z,\Delta\omega) = \frac{s}{2\sqrt{a\cdot(1-iks^2/2f)}}\exp[-\frac{(x-b)^2}{4a}+i\cdot\frac{k\cdot\alpha\cdot\Delta\omega}{f}x+c], \tag{2}$$

where

$$a = \frac{f_1^2}{k^2s^2} - i\cdot\frac{z-f_1^2/f}{2k}, \tag{2-1}$$

$$b = \alpha\cdot\Delta\omega\cdot(1-\frac{z}{f}), \tag{2-2}$$

$$c = i\cdot\frac{k\cdot\alpha^2\Delta\omega^2}{2f^2}(z-f), \tag{2-3}$$

$$f_1^2 = f^2\cdot\frac{k^2s^4}{4f^2+k^2s^4}. \tag{2-4}$$

The simultaneous temporal and spatial focused beam amplitude $A_2(x,z,t)$ is obtained by summing up the contributions over all $\Delta\omega$,

$$A_2(x,z,t) = \int_{-\infty}^{+\infty} M(x,z,\Delta\omega)\cdot\exp(-\frac{\Delta\omega^2}{\Omega^2}+i\Delta\omega t)\cdot d\Delta\omega$$

$$\approx \frac{s\cdot\Omega}{2}\sqrt{\frac{\pi}{m\cdot a|_{k=k_0}\cdot(1-ik_0s^2/2f)}}\cdot\exp[-\frac{x^2}{4a|_{k=k_0}}-\frac{(\Omega\cdot t+n\cdot x)^2}{4m}], \tag{3}$$

where

$$m = 1+\frac{\alpha^2\Omega^2\cdot(z-f)^2}{4f^2\cdot a|_{k=k_0}} - i\cdot\frac{k_0\cdot\alpha^2\Omega^2\cdot(z-f)}{2f^2}, \tag{3-1}$$

$$n = \frac{k_0\cdot\alpha\Omega}{f}+i\cdot\frac{\alpha\Omega\cdot(z-f)}{2f\cdot a|_{k=k_0}}. \tag{3-2}$$

Note that in the derivation of Eq. (3), we have neglected the dependence of the wave vector $k = k_0 + \Delta\omega/c$ on $\Delta\omega$, i.e., replaced every k with k_0, which is the value corresponding to the center frequency of the input spectrum. This approximation is valid for the 100-fs pulses typically used in MPM because the spectral bandwidth of the pulse is a small fraction of the carrier frequency.

From Eq. (3), the FWHM pulse width τ is found to depend only on the propagation distance z,

$$\tau(z) = \frac{1}{\sqrt{\mathrm{Re}[1/m]}}\cdot\frac{2\sqrt{2\ln 2}}{\Omega}. \tag{4}$$

Since the smallest value for m (i.e., $m=1$) is attainable only at the position $z=f$, the pulse width will be the shortest at the focal point. Note that the FWHM pulse width of $2\sqrt{2\ln 2}/\Omega$ at the focal point is the transform-limited value for a Gaussian spectrum with a FWHM bandwidth $\sqrt{2\ln 2}\cdot\Omega$, indicating that the pulse at the focal point is chirp-free. At distances outside of the focal point, *m* becomes a large complex number. Thus, the temporal pulse width increases quickly and the pulse is highly chirped. Therefore, the effect of simultaneous spatial and temporal focusing is realized.

#6020 - $15.00 US Received 16 December 2004; revised 23 February 2005; accepted 14 March 2005

3. Experiment and results

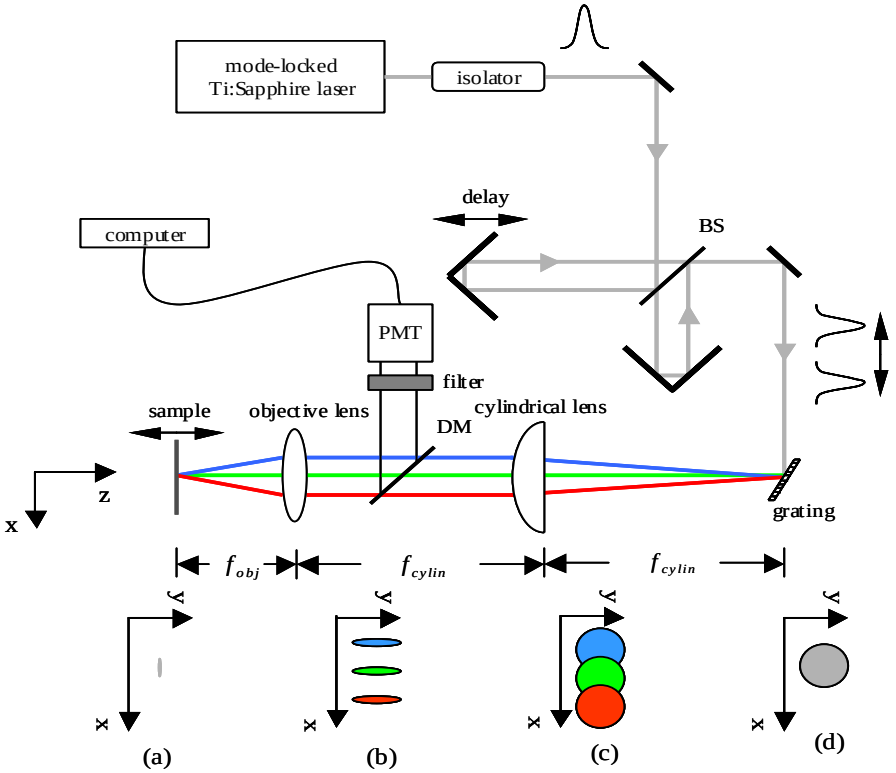

Fig. 2. Experimental setup for simultaneous temporal and spatial focusing and measurement of the pulse width dependence by second order auto-correlation. BS: beam splitter. DM: dichroic mirror. The input pulse train at 800nm center wavelength was generated by a mode-locked Ti:Saphire laser (Tsunami, Spectra-Physics). An isolator was used to overcome the instability caused by optical feedback. To spatially separate the spectral components, a reflective grating (1200 lines/mm) was used. The distances between the optical components are indicated. The insets show the cross section profiles of the laser beam impinging on the grating (d), at the back aperture of the cylindrical lens (c), at the back aperture of the objective (b), and at the focal plane of the objective (a). Note that the y-axis is pointing perpendicularly into the paper.

To demonstrate the simultaneous temporal and spatial focusing technique and support the intuitive picture as well as the theoretical analysis presented in the above sections, experimental work has also been carried out. The setup for the experiment is illustrated in Fig. 2. The required parallelly separated and chirp-free input rainbow beam was generated by first divergingly separate the different spectral component from a mode-locked Ti:Sapphire laser using a reflective grating and then recollimate them using a cylindrical lens. Note that the geometric dispersion caused by the grating is automatically canceled after the process of recollimation and therefore the rainbow beam after the cylindrical lens is chirp-free in spectrum. The simultaneous temporal and spatial focusing effect was then realized by passing the rainbow beam through an objective lens. The size of the rainbow beam is designed to under-fills the back aperture of the objective lens. Thus, negligible attenuation will be introduced to the rainbow edge. In our experiment, because the separation between the objective and the cylindrical lens was adjusted to be the focal length of the cylindrical lens, the Gaussian beam profile for each monochromatic component was therefore spatially transform-limited at the back aperture of the objective lens. As a result, the real number assumptions for both Ω and s used in our theory are consistent with our experiment Note that our setup appears to be similar to the basic building block in ultrafast optics technology for pulse compression and shaping, however, the pair of lens used in our setup does not form a well-known telescope 4-f system.

#6020 - $15.00 US Received 16 December 2004; revised 23 February 2005; accepted 14 March 2005

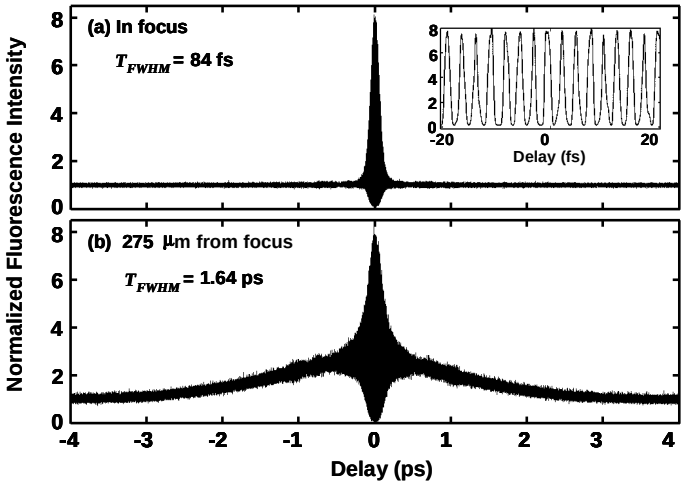

Fig. 3. Auto-correlation traces of the measured pulse at different sample positions: (a) at the focal plane of the objective, (b) when moved 275 μm away from focal plane. The inset inside trace (a) shows the interference fringes at the vicinity of zero time delay.

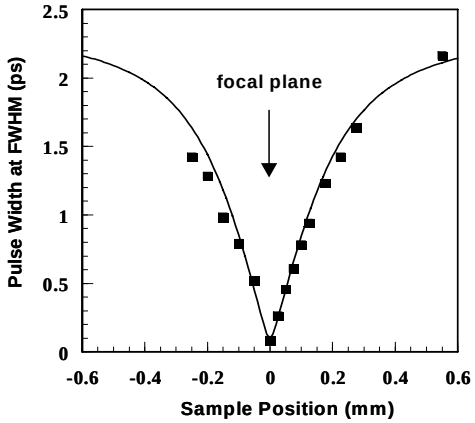

Fig. 4. Measured (solid square) and theoretically fitted (line) pulse width as a function of sample position. The location of the focal plane of the objective lens is set to be zero.

We measured the evolution of the temporal pulse width along the propagation direction in an interferometric second order autocorrelator which uses two-photon excited fluorescence of a thin Rhodamine sample as the nonlinear element [8]. The autocorrelation traces at the focal plane and far away from the focus are shown respectively in Fig. 3(a) and (b). At 275 μm away from the focus (Fig. 3(b)), a 1.64-ps pulse was measured and the characteristics of the interferometric autocorrelation trace were indicative of a highly chirped pulse. At the focal plane of the objective lens, however, a nearly chirp-free pulse was obtained and the measured 84-fs pulse width (Fig. 3(a)) is close to the original laser output. Fig. 4 shows the measured temporal pulse width (solid squares) at various distances away from the focal plane by translating the thin Rhodamine B sample. Our measurements indicated that a value of 25 for the pulse width stretching factor (PWSF), which is defined as the ratio between the pulse width measured at the back aperture of the objective lens and the pulse width measured at the focal point, could be achieved using the current setup. Using the model described in the theory section, a fitting curve for the pulse width (Eq. (4)) is also plotted in Fig. 4. The parameters used in the theoretical fit are s =0.1 mm, α =1.44 · 10^{-13} mm/Hz, and Ω =1.5 · 10^{13} Hz. From these numbers, the theoretical PWSF is calculated to be 21.6 which is slightly smaller than the measured one. The difference between the calculated and measured data is believed to be

#6020 - $15.00 US Received 16 December 2004; revised 23 February 2005; accepted 14 March 2005

caused by the fact that the theory is based on Gaussian profiles while the experiment is performed with Sech-like pulses.

3. Discussion

Because nonlinear excitation strongly depends on the excitation temporal pulse width, the temporal pulse width focusing shown in Fig. 4 can be used in multiphoton imaging to significantly reduce the out-of-focus background and improve the SBR performance. The most important parameter in determining the SBR improvement is PWSF. From Eq. (4), an analytical result for the PWSF is obtained as,

$$PWSF = \sqrt{1+\frac{\alpha^2\Omega^2}{s^2}} \approx \left.\frac{\alpha\cdot\Omega}{s}\right|_{\alpha\cdot\Omega>>s}. \quad (5)$$

Obviously, a larger PWSF leads to a better the SBR improvement. Since $\alpha\cdot\Omega$ is the size of the rainbow beam and s is the size of the monochromatic Gaussian beam (both measured at the back aperture of the objective), PWSF can be then intuitive understood as the beam expansion ratio due to the spatial separation of spectral components caused by the grating and cylindrical lens.

While such a reduction in background excitation will be valuable for imaging applications in general, we believe the demonstrated simultaneous spatial and temporal focusing will be particularly beneficial for imaging deep into scattering biological tissues, where background excitation fundamentally limits the penetration depth of optical imaging. At the present stage, the reported study is applicable to the case of a line-scanning system [9], which is typically used to obtain a fast frame acquisition rate. It is well-known that the excitation is not well localized longitudinally in a conventional two-photon line-scanning system, leading to a poor SBR. The demonstrated spatial and temporal focusing technique significantly enhances the SBR in a two-photon line scanning system, achieving characteristics similar to a conventional two-photon point-scanning system.

We note that the demonstrated spatial and temporal focusing technique significantly improves the SBR of the excitation, however, it does not address the detection path of a line-scanning system, which faces the well-known image smearing problem in any scattering tissue environment. Additional efforts will be needed in the future to address the detection difficulties in a line-scanning system so that the full potential of the technique can be utilized.

4. Conclusion

We have demonstrated the concept of simultaneous spatial and temporal focusing of femtosecond pulses. A pulse width stretching factor of 25 is obtained using a grating and a cylindrical lens. Based on the paraxial approximation, an analytical model for the temporal focusing is developed and supported by the measured data. Our technique can be applied to reduce the background excitation in two- or three-photon imaging and is highly promising for improving the penetration depth of optical imaging in scattering biological tissues.

Acknowledgment

The authors acknowledge valuable discussions with Dr. W. W. Webb. Chris Xu acknowledges initial discussions of the concept with Dr. Winfried Denk when they were both at Bell Laboratories, Murray Hill, NJ.

#6020 - $15.00 US Received 16 December 2004; revised 23 February 2005; accepted 14 March 2005